small
NANO MICRO

Orthogonal Cell-Based Biosensing: Fluorescent, Electrochemical, and Colorimetric Detection with Silica-Immobilized Cellular Communities Integrated with an ITO–Glass/Plastic Laminate Cartridge

Jason C. Harper, Thayne L. Edwards, Travis Savage, Svetlana Harbaugh, Nancy Kelley-Loughnane, Morley O. Stone, C. Jeffrey Brinker, and Susan M. Brozik**

This is the first report of a living cell-based environmental sensing device capable of generating orthogonal fluorescent, electrochemical, and colorimetric signals in response to a single target analyte in complex media. Orthogonality is enabled by use of cellular communities that are engineered to provide distinct signals in response to the model analyte. Coupling these three signal transduction methods provides additional and/or complementary data regarding the sample which may reduce the impact of interferants and increase confidence in the sensor's output. Long-term stability of the cells was addressed via 3D entrapment within a nanostructured matrix derived from glycerated silicate, which allows the device to be sealed and stored under dry, ambient conditions for months with significant retention in cellular activity and viability (40% viability after 60 days). Furthermore, the first co-entrapment of eukaryotic and bacterial cells in a silica matrix is reported, demonstrating multianalyte biodetection by mixing disparate cell lines at intimate proximities which remain viable and responsive. These advances in cell-based biosensing open intriguing opportunities for integrating living cells with nanomaterials and macroscale systems.

1. Introduction

Advances in agriculture and foodstuff production have sustained the current rate of world population growth, but have lead to an enormous increase in the use of pesticides and herbicides, with clear implications towards environmental and human health.[1,2] Analytical devices capable of detecting chemicals in the environment with high specificity

Dr. J. C. Harper, Dr. T. L. Edwards, Dr. S. M. Brozik
Biosenors & Nanomaterials
Sandia National Laboratories
PO Box 5800, Albuquerque, NM 87185, USA
E-mail: smbrozi@sandia.gov
T. Savage
Chemical & Nuclear Engineering
University of New Mexico
1001 University Blvd S.E., Ste. 100
Albuquerque, NM 87106, USA

DOI: 10.1002/smll.201200343

Dr. S. Harbaugh, Dr. N. Kelley-Loughnane,
Dr. M. O. Stone
Applied Biotechnology Branch
Human Effectiveness Directorate
Air Force Research Laboratory
Dayton, OH 45433, USA
Dr. C. J. Brinker
Self-Assembled Materials, Sandia National Laboratories
Chemical & Nuclear Engineering
Molecular Genetics & Microbiology
University of New Mexico
1001 University Blvd S.E., Ste. 100, Albuquerque, NM 87106, USA
E-mail: cjbrink@sandia.gov

and sensitivity are essential for regulatory purposes and for advancing our ability to identify, understand, and enable remediation of environmental pollutants. Additionally, such devices could prove valuable in food safety, medicine, public safety, and military defense applications.[3] Thus, demand for analytical devices that are robust, inexpensive, portable, low-power and simple to operate, continues to dramatically increase.

As an alternative to traditional chemical and physical analysis techniques, analytical tools based on living cells to provide analyte recognition and response functions are attracting increased attention.[4] Often described as the equivalent of canaries used to detect toxic gases in mines,[5] whole cell-based biosensors have proven effective in the non-specific detection of various cellular stresses, DNA damage, and general toxicity.[6,7] Additionally, living cells are capable of amplifying subtle signals by many orders of magnitude via native signaling cascades. Used together with advances in genetic engineering, real-time and highly sensitive and specific cell-based detection of bacteria, viruses, and toxins has been reported.[8]

Living cell-based biosensors, however, suffer from several limitations including i) difficulties in interfacing cells with the transducer, effectively hindering translation of the biological response to a measurable signal,[4] ii) susceptibility of cells to stresses from the ex vivo environment leading to a high false positive/negative response rate[9] or loss in viability/activity,[10] and iii) interferences with complex sample solutions. Depending on one's method of signal transduction, common interferants include molecules that are redox active at the potential range employed for electrochemical measurements,[4] or are autofluorescent or cause high solution turbidity, confounding optical measurements.[1] To address limitations associated with interference and ambiguous readings, use of a device that relies on more than one distinct method for signal transduction may prove an innovative option. Coupling the two most commonly used signal transducers in cell-based biosensing, electrochemistry and fluorescence, would provide complementary information regarding the sample properties, substantially decreasing false positive/negative responses due to interferants, and significantly increasing the confidence of the analyst in the results.

Indeed, platforms capable of simultaneous amperometric and fluorescence measurements of cells,[11] and most recently, simultaneous amperometric and total internal reflection fluorescent (TIRF) measurements,[12] have been reported. In these pioneering works exocytosis from chromaffin cells was monitored under conditions of continuous perfusion culture. Although ideal for fundamental molecular biology studies performed over several hours these, and other similar devices,[13–15] were not designed for long-term cell-based environmental biosensing. In another recent study, the utility of coupling electrochemical and fluorescent techniques for cell-based biosensing of pesticides was reported.[16] In that work photosynthetic cells were entrapped within protein gels in two separate devices, one for fluorescence measurements, the other for amperometric measurements. The authors showed that coupling these two data sets provided less ambiguous identification of target toxins.

Herein we report the first orthogonal detection mode living cell-based sensor capable of fluorescent, electrochemical, and colorimetric measurements of a target analyte in complex media, all on a single device. Orthogonal cell-based biosensing is enabled by simultaneous use of multiple cell lines engineered to provide distinct responses to the target analyte and multiple electrodes for sensing. We also address sensitivity of the cells to the environment via entrapment in a matrix derived from glycerated silicate, which we have recently characterized for cell-based sensing applications.[17] Finally, we report what we believe to be the first co-entrapment of eukaryotic and bacterial cells in a silica matrix, demonstrating multianalyte biodetection by mixing cell lines of varying functional ability.

2. Results and Discussion

2.1. Fabrication of the ITO–Glass/Plastic Laminate Cartridge

Fabrication of the senor platform's fluidic cartridge was accomplished via laser machining of plastic laminates.[18] The device was composed of nine thin plastic layers, each cut with a CO_2 laser, and an indium tin oxide (ITO)-coated microscope slide patterned by photolithography and wet chemical etching. A schematic layer-by-layer representation of the ITO–glass/plastic laminate cartridge is shown in **Figure 1**a, with an expanded layer-by-layer schematic presented in the Supporting Information (SI; Figure S1). Adhesive coatings on plastic layers allowed for assembly of the device by simple hydraulic pressing of the layers. Fabrication details can be found in the Experimental Section.

A photograph of the assembled cartridge is shown in Figure 1b. Visible in the image are the ITO leads and the array of 3 electrochemical cells, each containing 3 individually addressable electrodes at the bottom of each well. Surface areas of the ITO working, pseudo-reference, and counter electrodes are 22.9, 8.2, and 55.1 mm^2, respectively. A schematic of the assembled cartridge highlighting the conductive electrode regions is presented in Figure S2 (SI). The cross-section view through one of the wells (Figure 1c) highlights the region in which cells entrapped in a glycerol–silica matrix thin film are interfaced between the ITO electrode surface and a polymethylmethacrylate (PMMA) sheet (Figure 1a and Figure S1 (SI), layer 4, pink). The portion of this PMMA sheet that forms the well bottom is porous, allowing the analyte solution to access the underlying silica matrix entrapped cells. A removable seal (layer 5, yellow) is placed over the porous well bottoms during assembly (Figure 1c). Living cells in a glycerol–silica matrix precursor solution are introduced to the device through microfluidic ports on either side of each well. Following introduction of the cell/glycerol–silica matrix solution, the inlet and outlet ports are sealed with adhesive tape. In this configuration, the device can be stored under ambient conditions for months with significant retention in cellular activity and viability (40% viability after 60 days).

NANO MICRO small

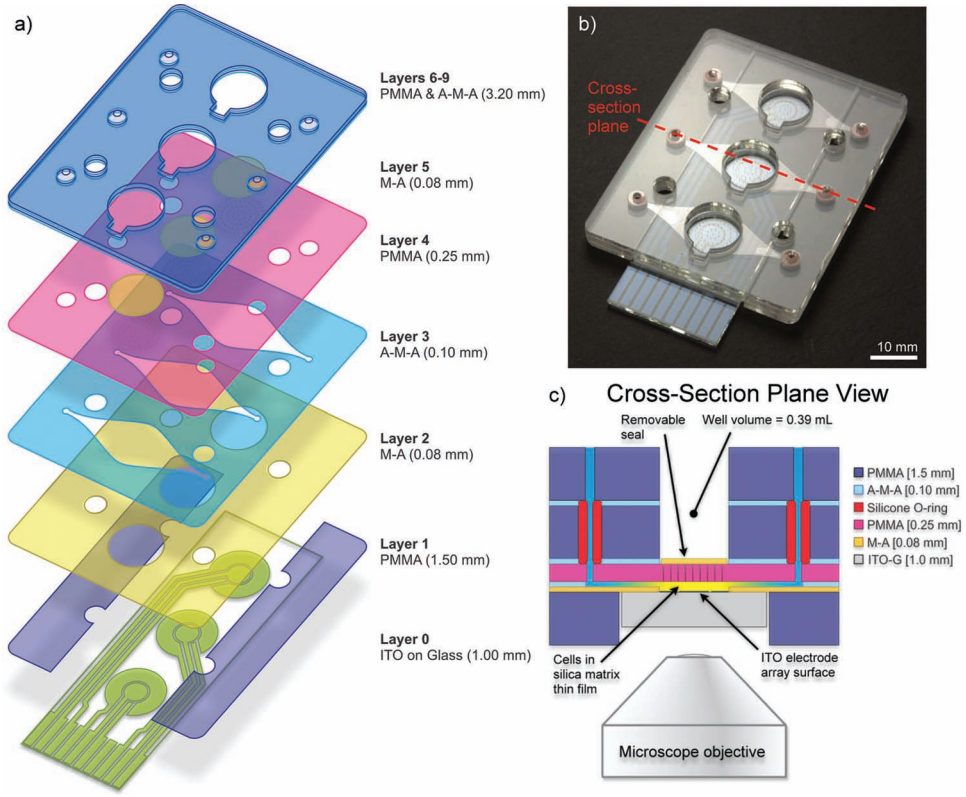

Figure 1. a) Schematic layer-by-layer representation and b) photograph of the ITO–glass/plastic laminate cartridge. Fluorescence and visible detection occur through the glass, ITO, and silica matrix; electrochemical detection is performed on the ITO surface. c) Cross-section cutout schematic of the device (from the plane marked in panel (b)) highlighting the location of living cells encapsulated within the glycerol–silica matrix thin film (bright yellow). Blue represents fluidic access vias through the o-rings and the fluidic channel over the ITO electrode array for introducing the cell/silica matrix solution to the cartridge. Pores were laser machined into portions of PMMA layer 4 (pink) directly above the electrodes, providing analyte solution access to the underlying entrapped cells upon removal of the Mylar seal at the bottom of the well (layer 5, yellow). Abbreviations: polymethylmethacrylate (PMMA), polyethyleneterapthalate (Mylar, M), indium tin oxide (ITO), glass (G), Mylar coated with adhesive oriented down (M-A), Mylar coated with adhesive on both sides (A-M-A).

2.2. Co-encapsulation of Engineered Cellular Communities

Orthogonal detection mode cell-based biosensing was enabled by co-immobilization of multiple cell lines engineered to provide distinct responses to a target model analyte. An equal molar mixture of *S. cerevisiae* cells engineered to express yellow fluorescent protein (YFP), and *S. cerevisiae* cells engineered to express and secret glucose oxidase (GOx), were integrated within a glycerol–silica matrix thin film in an ITO–glass/plastic laminate cartridge. Expression of YFP and GOx in each cell line was induced by the presence of a model analyte, galactose. Detection of YFP occurred via fluorescence microscopy imaging through the transparent ITO electrodes and silica matrix. Electrochemical detection occurred at the ITO electrode via chronoamperometric reduction of hydrogen peroxide (H_2O_2) produced from turnover of expressed GOx using a hand-held potentiostat.

2.3. ITO Working Electrode Functionalization and Characterization

H_2O_2 electrochemistry is unfavored on ITO surfaces. To enhance the amperometric response from H_2O_2 reduction while maintaining an optically transparent surface facilitating fluorescence measurements, the ITO surface was functionalized with gold nanoparticles (AuNPs), followed by AuNP-catalyzed electroless Prussian blue (PB) deposition. Electrode surface functionalization was performed within the fully assembled device and was selective, modifying the working electrode (WE) only. AuNPs were deposited from a solution of potassium gold cyanide onto the ITO working electrode (see Experimental Section). Following electrodeposition, the AuNP-modified ITO surface changed from a dull brown to a light pink, as shown in **Figure 2**a. This characteristic color shift is due to surface plasmon resonance coupling of the deposited AuNPs. Scanning electron microscopy (SEM) images of the bare ITO surface, and the ITO–AuNP surface, are shown in Figure 2b and c, respectively. Images reveal mostly spherical AuNPs evenly distributed across the ITO surface with diameters from 10 to 75 nm, with larger particles being more globular in structure.

Cyclic voltammograms in H_2SO_4 solution prior to and after AuNP deposition are shown in Figure 2e. The current response from a bare ITO electrode (blue trace) was nearly flat, as expected for a clean ITO surface. Following AuNP deposition (red trace), an oxidation wave centered near 845 mV (versus (vs.) ITO pseudo-reference), and reduction

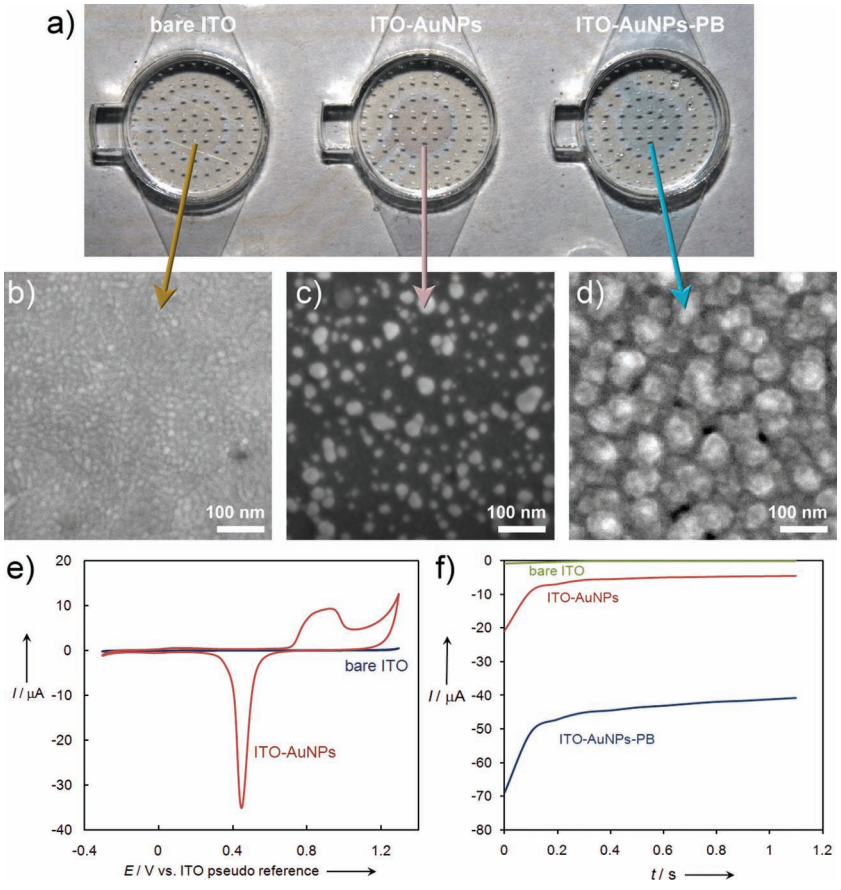

Figure 2. a) Photograph of an ITO–glass/plastic laminate cartridge with a bare ITO WE (left, light brown), a AuNP-modified ITO WE (middle, light pink), and a AuNP–PB-modified ITO WE (right, dull blue). Image brightness, contrast, and leveling were adjusted to improve color distinction between WEs. SEM images (b–d) of the WEs imaged in panel (a): b) bare ITO, c) AuNP-modified ITO, and d) AuNP–PB-modified ITO. e) Cyclic voltammograms (CV) of a bare ITO (blue) and a AuNP-modified ITO (red) electrode in an ITO–glass/plastic laminate cartridge in 1 M H_2SO_4, $v = 100$ mV s^{-1} (second CV sweeps shown). f) Chronoamperometric response of a bare (green), a AuNP-modified (red), and a AuNP–PB-modified (blue) ITO WE in 1 mM H_2O_2, 1× phosphate buffered saline (PBS), pH 7.4. $E = -100$ mV vs. on-chip ITO pseudo-reference.

peak at 455 mV, were observed. These waves are attributed to oxygen absorption and desorption, respectively, on the AuNP surface. Integration of the reduction wave provides the total charge transferred upon oxygen desorption, which is directly proportional to the electroactive surface area of Au, according to the relation of 400 µC cm^{-2}.[19] The charge measured from the reduction wave shown in Figure 2e was 7.49 µC which corresponds to a AuNP electroactive surface area of 1.875 mm^2. This accounts for less than 8% of the ITO working electrode surface area, which thus retained excellent optical transparency.

Following AuNP modification of the ITO working electrode, the surface was functionalized with PB ($Fe_4^{III}[Fe^{II}(CN)_6]_3$). Often described as an "artificial peroxidase," PB can significantly enhance H_2O_2 reduction while being more stable than enzymes used for the same purpose.[20] Incubation of the 3 electrode cell surface with a solution of $FeCl_3$, $Fe(CN)_6^{3-}$, KCl, and HCl (see Experimental Section) resulted in deposition of PB onto the ITO–AuNP working electrode only. A characteristic change in color to dull blue was observed for the working electrode, as shown in Figure 2a. The following mechanism was proposed by Neff and co-workers[21] for electroless deposition of PB onto metallic substrates from a ferric ferricyanide solution:

$$Fe^{3+} + \tfrac{1}{2}H_2O = \tfrac{1}{4}O_2 + H^+ Fe^{2+} \quad (1)$$

$$K^+ + Fe^{2+} + Fe(CN)_6^{3-} = KFe^{III}[Fe^{II}(CN)_6] \quad (2)$$

The reduction of free ferric ions, or ferric ions in the associated complex, as shown in reaction (1), is thermodynamically unfavorable due to the standard free-energy change of +173 kJ/mol. The overall driving force could be provided by the subsequent formation of PB according to reaction (2); the total standard free energy change for the combined reaction is –177 kJ/mol. Neff and co-workers further proposed that Au or Pt substrates can act as catalysts for reaction (1), which is also supported by recent reports of electroless PB deposition onto AuNPs[22] and PtNPs[23] from solutions of Fe^{3+} and $Fe(CN)_6^{3-}$. SEM images of the ITO–AuNP–PB surface reveal a facetted microstructured network, characteristic of the microcrystalline structure of PB,[20] with features on the order of 100 nm in diameter (Figure 2d). The resultant ITO–AuNP–PB surface also retained excellent optical transparency allowing for fluorescence measurements of YFP expressing *S. cerevisiae* cells through the functionalized electrodes.

The current response following a 1 s potential step to –100 mV (vs. ITO pseudo-reference) for each of these surfaces in 1× PBS containing 1 mM H_2O_2 is shown in Figure 2f. A significant increase in H_2O_2 reduction current was observed for the ITO–AuNP–PB surface (blue trace) vs. the ITO–AuNP (red trace) and bare ITO (green) trace, with currents of –50.9, –9.1, and –0.4 µA, respectively (200 ms from potential step initiation). The current from H_2O_2 reduction obtained from the ITO–AuNP–PB surface was sufficient to allow detection of H_2O_2 generated by GOx expressed and secreted by *S. cerevisiae* cells used in this study.

2.4. Orthogonal Cell-Based Electrochemical, Fluorescent, and Colorimetric Detection

A solution of complex media (YP, see Supporting Information) containing galactose (2% mass) was added to a well in the ITO–glass/plastic laminate cartridge, following removal of the plastic cap (layer 5), to an end volume of 250 µL. Cells

NANO MICRO small

entrapped beneath the well were then monitored via simultaneous fluorescence microscopy and chronoamperometry measurements. The electrochemical and fluorescence response with time is shown in **Figure 3**a. The amperometric response (blue trace) initially increased more rapidly than the fluorescence response (red trace), reaching a signal 3σ above the negative control signal in less than 4 h. This same fluorescence signal intensity (3σ above the negative control) took nearly 6 h to develop. This is not unexpected as the electrochemical response is based on catalytic production of H_2O_2 by GOx, whereas the fluorescent response is proportional only to the total concentration of YFP expressed by the cells (not catalytic). Between 6–9 h from introduction of the analyte sample, the electrochemical response reached a maximum, after which the signal continued to decrease with time. This is attributed to the depletion of enzymatic substrate, and the breakdown and electrochemical consumption of H_2O_2. In contrast, the fluorescent signal continued to increase, reaching a maximum between 12–18 h from induction. This fluorescent signal was highly stable, being detectable even after cell death (data not shown). Of note is the 1 h delay in development of fluorescence signal 3σ above the negative control from our previously reported study.[17] Preferential metabolism of glucose in the complex medium may account for this initial delay in uptake and response to galactose. However, there was no statistically significant change in the time to reach maximum signal, or in the fluorescent signal intensity. Further, slight variation in initial response time (≤±7%) between cultures of *S. cerevisiae* (as well as *E. coli*) was observed and can be reasonably attributed to variation between colonies used for inoculation and initial culture conditions.

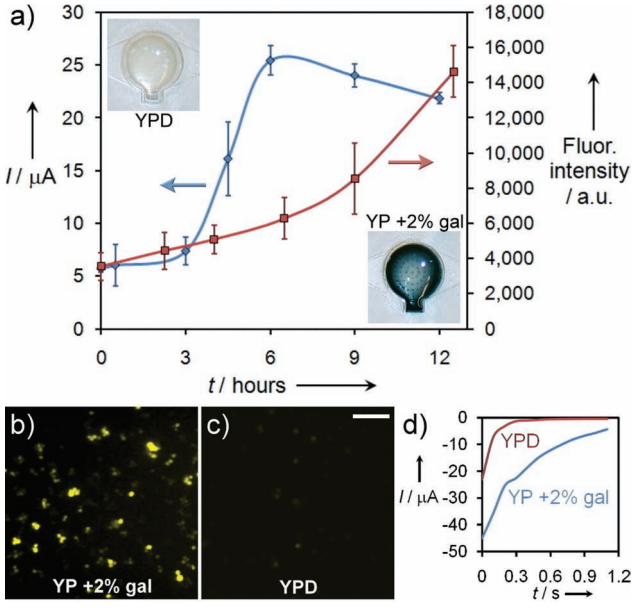

Figure 3. Orthogonal biosensing of a single model analyte via fluorescent, electrochemical, and visible (colorimetric) detection modes. *S. cerevisiae* cells engineered to express either YFP or GOx in response to galactose (gal) were co-encapsulated in a glycerol–silica matrix thin film within an ITO–glass/plastic laminate cartridge. a) Simultaneous electrochemical (blue) and fluorescence (red) measurements upon treatment with YP +2% gal +50 mM glucose at 30 °C. Error bars are the standard deviation of 3 independent measurements. Insets: Photographs of colorimetric assay results following overnight incubation of wells with YPD (negative control) or YP +2% gal at 30 °C. Fluorescence microscopy images (b,c) of YFP expression following an overnight treatment with b) YP +2% gal or c) YPD at 30 °C. (False-colored, scale bar = 30 μm). d) Chronoamperometric measurements of H_2O_2 produced by GOx turnover following treatment with YPD (red) or YP +2% gal (blue) for 9 h at 30 °C.

Typical fluorescent and amperometric responses to treatment with galactose in complex media are shown in Figure 3b and d, respectively. Bright fluorescence was observed for glycerol–silica matrix encapsulated cells in an ITO–glass/plastic laminate cartridge treated with YP +2% gal (Figure 3b). A similar response was also observed electrochemically. The current response 200 ms after a potential step to –100 mV was 35.6 μA for encapsulated cells in an ITO–glass/plastic laminate cartridge treated with YP +2% gal. The high selectivity of the engineered stains for galactose over the monosaccharide epimer, glucose (negative control), in complex media is shown in Figure 3b and d. Encapsulated cells treated with YPD (2% glucose) showed very little background fluorescence (Figure 3c), and only 7.2 μA of electrochemical signal was recorded 200 ms after a potential step to –100 mV. These results show the significant selectivity possible from this cell-based sensing device within an environmentally relevant and potentially confounding matrix. Use of media to introduce the target, however, is not required; statistically identical responses to the target analyte in complex media, phosphate buffer, or minimal salt solutions were measured.

The galactose concentration dependence of amperometric and fluorescent signals was also measured and is presented in **Figure 4**. The dynamic ranges for both amperometic (Figure 4a) and fluorescent (Figure 4b) responses were similar, spanning 4 orders of magnitude with saturating signals measured for concentrations above 0.2% mass (10 mM) galactose. The limit of detection for both fluorescence and amperometric measuments was defined by the lowest signal of a positive control whose signal strength was greater than the sum of the mean signal of a negative control sample (μ) and its standard deviation (σ) multiplied by 3 (LOD = $\mu + 3\sigma$). For amperometric and fluorescence measurements the LOD was 6 and 22 μM, respectively. This response is typical of that reported for other cell-based biosensors relying on target analyte induced expression of reporter proteins.[7,24,25] No significant chip-to-chip variation in response time or concentration dependence was observed. For devices operated at room temperature (22 °C) an approximately 15% increase in response time to obtain a signal 3σ above background was observed in comparison to devices operated at 30 °C. The most significant source of measured variation was the time for individual cells within the integrated population to begin expression of the reporter protein. This variation is attributed to heterogeneity of cell phase, metabolic activity, and gene expression within the cell population.

Colorimetric detection of galactose from YFP and GOx expressing *S. cerevisiae* cells entrapped in an ITO–glass/plastic laminate cartridge was also demonstrated (Figure 3a, insets). Colorimetric assay solution (ABTS (2,2′-azino-bis[3-ethyl-benzothiazoline-6-sulfonic acid]) assay, see Experimental Section) was added to each well following a 9 h

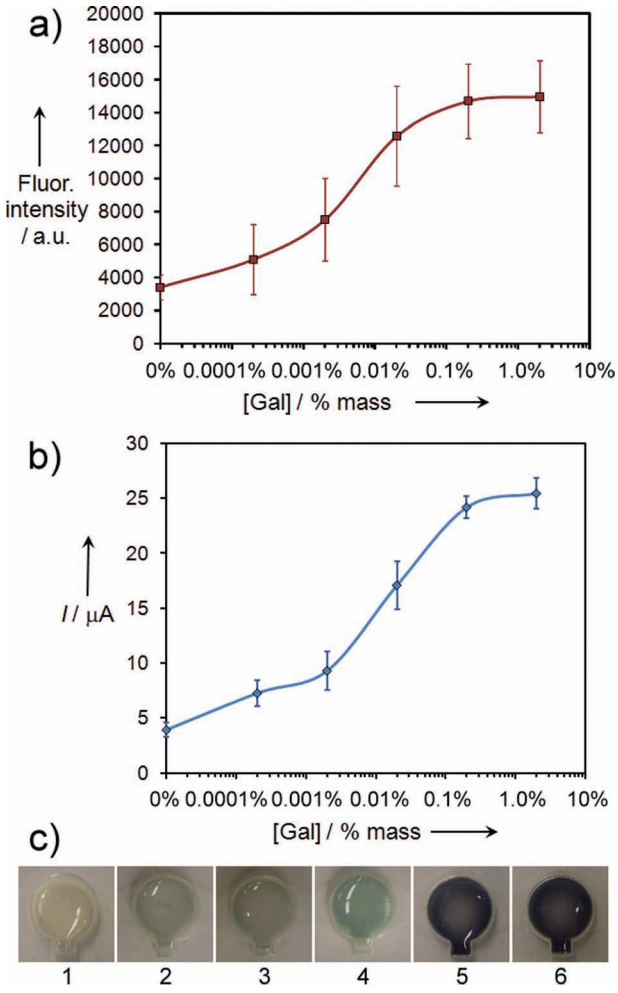

Figure 4. a) Fluorescence intensity and b) chronoamperometric current response from glycerol–silica matrix encapsulated *S. cerevisiae* cells in a ITO–glass/plastic laminate cartridge following treatment with YP +2%, 0.2%, 0.02%, 0.002%, 0.0002% gal, and YPD (0% gal control containing 2% glucose) at 30 °C overnight (a), or 9 h (b). Error bars are the standard deviation of 3–5 independent measurements. c) Photographs of ITO–glass/plastic laminate cartridge wells following an overnight ABTS assay at room temperature (22 °C). Glycerol–silica matrix encapsulated *S. cerevisiae* cells were previously exposed to: 1) YPD (0% gal, 2% glucose), 2) YP +0.0002% gal, 3) YP +0.002% gal, 4) YP +0.02% gal, 5) YP +0.2% gal, and 6) YP +2% gal for 9 h at 30 °C.

incubation with YPD or YP +2% gal. After overnight colorimetric assay, the assay solution and silica matrix remained clear in the well treated with YPD. In the well treated with YP +2% gal, the assay solution and silica matrix developed a strong dark green-blue color that was clearly discernable by eye. This provides an additional orthogonal approach for the detection of the target analyte that can be performed and measured without any instrumentation or power, significantly simplifying leave-behind environmental monitoring. Photographs and absorbance measurements for ABTS assays following incubation with YP containing differing concentrations of galactose are presented in Figure 4c and Table S1 (SI).

2.5. Co-encapsulation of Eukaryotic and Bacterial Cells, and Multianalyte Detection

We further demonstrated the ability to co-entrap disparate classes of living cells within an ITO–glass/plastic laminate cartridge. In this case, eukaryotic *S. cerevisiae* cells engineered to express YFP in the presence of galactose, and gram-negative prokaryotic *E. coli* "riboswitch" cells, were co-immobilized in a glycerol–silica matrix thin film. As an improvement to our earlier fluorescence resonance energy transfer (FRET) based riboswitch construct,[26] the riboswitch *E. coli* system used in this work contains a synthetic riboswitch: an mRNA strand consisting of an aptamer sequence against the respiratory drug, theophylline, and a sequence encoding a new green fluorescent protein from amphioxus *Branchiostoma floridae* (GFPa1).[27] In the absence of theophylline, this mRNA strand forms a hairpin loop, preventing access to, and translation of, the GFPa1 sequence. In the presence of theophylline, the aptamer sequence binds the drug, exposing the GFPa1 sequence for translation, resulting in a strong GFP signal.

Multianalyte detection from the co-entrapped *S. cerevisiae* and *E. coli* cells is shown in **Figure 5**. Treatment of the cells in the cartridge with 2% galactose and/or 3.5 mM theophylline in complex medium (YP) resulted in strong YFP and/or GFP fluorescence. Fluorescence intensities and images of the responses clearly show the cell-based sensor successfully distinguished between the two targets. Also apparent is a slightly higher background signal for the YFP expressing *S. cerevisiae* cells which is attributed to "leaky promoter" expression in cells from stationary phase culture.[17] The lower GFP background obtained from the riboswitch *E. coli* cells is inherent of the tighter synthetic riboswitch-based regulation over fluorescence.[26] These results further demonstrate that both classes of disparate cells remain viable and active, even when immobilized together at intimate proximities within the glycerol–silica matrix.

Finally, the glycerated silicate based immobilization matrix chosen for this study provides for long-term stability of the entrapped cells. We have previous reported that use of this matrix with *S. cerevisiae* cells from stationary phase cultures could potentially allow "leave behind" environment monitoring sensors to operate for over 2 months, after which time the sensors can be collected, analyzed, and replaced.[17] Prokaryotic *E. coli* cells encapsulated within this matrix have also demonstrated similar long-term viability and activity to *S. cerevisiae* cells, with 54% viability and retained responsiveness to theophylline 43 days from encapsulation.

3. Conclusion

We have demonstrate the first orthogonal fluorescent, electrochemical, and colorimetric detection of a target analyte in complex media, with high specificity, using a single cell-based biosensing platform. Coupling these three signal transduction methods provides complementary information regarding the sample properties, potentially reducing the impact of interferants from complex samples, and substantially increasing the confidence of the analyst in the sensor's output. We also

NANO MICRO small

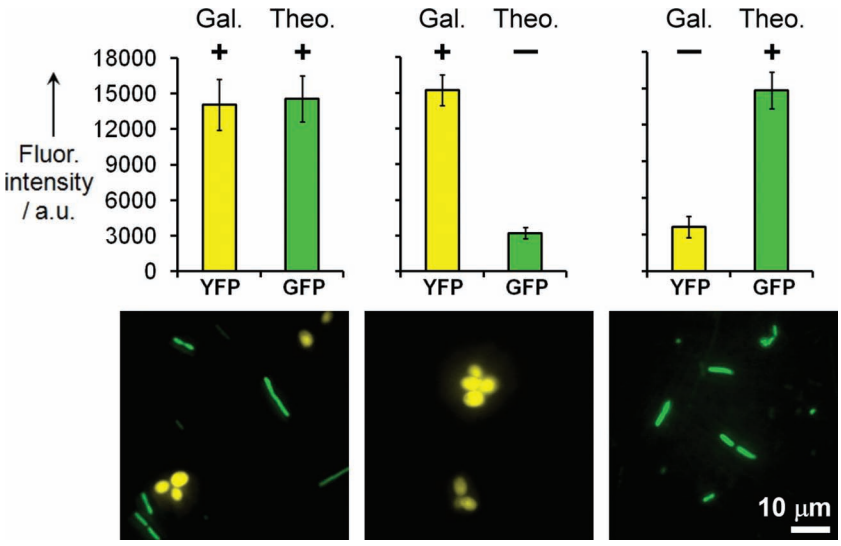

Figure 5. Multianalyte biodetection via co-encapsulation of eukaryotic and bacterial cells in a glycerol–silica matrix thin film within an ITO–glass/plastic laminate cartridge. Exposure of *S. cerevisiae* cells to galactose induces YFP expression. Exposure of *E. coli* 'riboswitch' cells to theophylline (theo.) results in GFP expression. Treatment in YP with (+) or without (–) 2% gal. and/or 3.5 mM theo. for 17 h at 30 °C. Fluorescence images are false-colored. Error bars are the standard deviation of 3 independent measurements.

showed the first co-entrapment in a silica matrix of eukaryotic and prokaryotic cells which remained viable and responsive, facilitating multianalyte measurements within the ITO–glass/plastic laminate cartridge. These advances in cell-based biosensing hold significant implications towards the development of practical devices for environmental monitoring and open intriguing opportunities for integrating living cells with nanomaterials and macroscale systems.

4. Experimental Section

Materials and Reagents: Aqueous solutions were prepared with 18 MΩ water using a Barnstead Nanopure water purifier (Boston, MA). Tetraethylorthosilicate (TEOS), glycerol (anhydrous), titanium isopropoxide (97%), potassium ferricyanide ($Fe(CN)_6^{3-}$), gold potassium cyanide ($Au(CN)_2$), glucose (99%), galactose (99%), potassium chloride (KCl), theophylline (99%), ampicillin sodium salt, peroxidase (from horseradish), and ITO-coated glass microscope slides (30–60 Ω/sq) were purchased from Sigma-Aldrich (St. Louis, MO). 2,2′-Azinobis [3-ethylbenzothiazoline-6-sulfonic acid]-diammonium salt (ABTS, 10 mg tablets), phosphate buffer saline (PBS) solution, pH 7.2 (11.9 mM phosphates, 137 mM NaCl, and 2.7 mM KCl at 1× concentration), sodium phosphate (monobasic and dibasic), 30% hydrogen peroxide (H_2O_2), hydrochloric acid (HCl), sulfuric acid (H_2SO_4), acetone, ammonium hydroxide, ferric chloride ($FeCl_3$) solution (40% w/v), and yeast extract were obtained from Fischer Scientific (Pittsburgh, PA). Bacto Peptone and Bactro Tryptone were from BD Biosciences. Difco Luria-Bertani (LB) was purchased from Becton Dickinson and Company (Sparks, MD). All reagents were used as received.

Culture Mediums and Cell Preparation: Yeast extract, peptone, dextrose (YPD) media contained yeast extract (10 g), Bacto peptone (20 g), and glucose (20 g) in nanopure water (1 L). In yeast extract, peptone, galactose (YP +2% gal) induction medium, glucose in the YPD recipe was replaced with galactose. In studies where the concentration of galactose was varied, the concentration of all other components (YP) remained constant. LB broth contained bactrotryptone (10 g), yeast extract (5 g), NaCl (10 g), and ampicillin (1 g) in nanopure water (1 L).

A single colony of *S. cerevisiae* was inoculated into YPD media (3 mL) in a 15 mL volume culture tube. This solution was cultured at 30 °C in a shaking incubator at 250 rpm until stationary phase (7–10 days). A single colony of *E. coli* was inoculated into LB media (35–40 mL) in a 250 mL flask. This inoculated solution was cultured in a shaking incubator at 250 rpm to stationary phase (18–24 h) at 37 °C.

Synthesis of Poly(Glycerol) Silicate (PGS):[17,28] A round-bottomed flask equipped with a stir bar, dropping funnel, and reflux condenser was charged with glycerol (63.4 g, 688 mmol) and heated to 60 °C with stirring. To the hot glycerol was added a mixture of TEOS (10.21 g, 49.0 mmol) and titanium isopropoxide (1.02 g, 3.0 mmol). After addition, the reaction mixture was refluxed at 130 °C for 3 h. Ethanol co-product was removed under vacuum (~10 mTorr) at 130 °C. The product (63.5g; 98% yield) was a viscose opalescent white liquid that was somewhat soluble with water. The mass of the product agreed with the reported theoretical formula: $Si(C_3H_7O_3)_4{\cdot}10C_3H_8O_3$; however, it is certain that many isomers exist in the mixture as well as some inadvertent hydrolysis products.

ITO–glass/Plastic Laminate Cell-Based Biosensing Cartridge: The ITO electrochemical cell sensor array was integrated into a plastic package which included microfluidic channels allowing a silica matrix thin film to be cast between the ITO electrode surface and the porous well bottom (390 mL volume). The integrated system is referred to as a cartridge with overall size of 5 mm × 50 mm × 75 mm, and is shown schematically in Figure 1a and Figure S1 and S2 in the SI. The cartridge was fabricated by laminating laser-cut layers of polyethyleneterapthalate (PET, Mylar) and polymethylmethacrylate (PMMA), and final adhesion to an ITO-coated glass microscope slide. The basic fluidic channel was made by cutting the channel pattern using a CO_2 laser ablation system (Model PLS 6.75 with a 60 watt cartridge, Universal Laser Systems, Scottsdale, AZ) into a custom sheet of PET double-side coated with pressure sensitive acrylic-based adhesive (0.05 mm thick for the PET and 0.025 mm thick for each adhesive; Fralock, Valencia, CA) forming the side walls and defining the channel's three dimensions. The top and bottom walls were formed from plain PET (0.1 mm thick). Into one or both of these plain PET sheets fluidic vias were cut to allow for access to external tubing or channels located above or below. Alignment of the layers was accomplished with registration holes and pins. The layers were pressed together between two flat steel plates in a hydraulic press.

Individually addressable working, pseudo-reference, and counter electrodes at the bottom of each well were defined by etching ITO through a photolithography defined photoresist mask.

The ITO electrodes were fabricated from commercially available ITO-coated glass microscope slides (part no. 636908, Sigma-Aldrich, St. Louis, USA). The ITO thickness was specified at 300–600 Å (30–60 Ω/sq.). AZ4110 positive tone photoresist was spin-coated onto the slide at 4000 rpm for 30 s and then baked on a hotplate at 90 °C for 90 s. The resist was exposed to a broad UV light source of 200 mJ/cm^2 and subsequently developed in AZ400k (5:1 dilution in deionized (DI) water) for 2 min. The ITO was etched in 18% hydrochloric acid for 5 min at room temperature. The photoresist mask was then removed using acetone and cleaned with an isopropanol and DI water rinse.

The fluidic fixture consisted of nine plastic laminate layers (four PMMA, five PET), an ITO-coated glass slide, and a set of O-rings. Each of these layers is numbered from zero to nine starting at the glass slide, and is shown in detail in Figure S1 (SI). In Figure 1 only layers 0–5 are shown exploded, without the O-rings, for simplicity. Layers 2, 3, 5, and 6 were PET with single- (M-A) or double-sided (A-M-A) adhesive. Layer 4 was 0.5 mm thick PMMA. Layers 0, 7, and 9 were 1.5 mm thick PMMA supports. Layer 7 housed six O-rings (silicone, AS568A-002, *McMaster-Carr*, Santa Fe Springs, CA) for receiving 1/16 inch diameter rigid PEEK or PTFE tubing to introduce and remove liquid samples at low pressures (tested to be leak free up to at least 90 psi) without the need for additional fittings. Electrical connections from the hand-held potentiostat to layer 0 were made using a 10-conductor card-edge connector and ribbon cable assembly (3M, St. Paul, MN).

The primary channel which delivered and contained the cells in sol–gel was located in layer 3 with dimensions of 100 μm thick and entrance/exit regions combined volume of 10 μL. Layer 2 defined the circular regions exposing the electrodes of layer 0 while masking the electrode leads. The depth of the circular region exposing the electrodes was 175 μm, with a total volume of 20 μL. The upper wall of the channel, layer 4, was made from PMMA. In this layer, located over the electrodes and at the bottom of the well, an array of 81 holes (approximately 50 μm in diameter) was laser ablated to form a "shower head" pattern. Prior to the introduction of the sol–gel the shower head was capped with PET layer 5. This prevented the cell/sol–gel precursor solution from leaking through the porous region of layer 4, and allowed for long-term storage of the entrapped cells under ambient conditions without evaporation. Prior to introducing the analyte solution to the cartridge well, the cap was removed to allow liquid reagents to be effused through the porous well bottom into the gel (locally over the electrodes) without disruption of the gel.

The laminates were assembled in the following order, starting with layer 8: 9, 7, 6, 4, 5, 3, 2, and 1. After the addition of one or more layers, they were pressed at approximately 3000 psi at room temperature for 2 min in a manual hydraulic laboratory press (Model 3850, *Carver, Inc.*, Wabash, IN). In the final step, layer 0 was pressed at a reduced pressure of 500 psi for 2 min to prevent cracking of the glass layer. A custom fixture, to ensure alignment of layers and uniform force distribution, was fabricated from two plates of 1/4 inch steel with surfaces machined and polished flat. Complete assembly of the cartridge from the prepared layers required 45 min.

Functionalization of ITO Working Electrodes with AuNPs and PB: Prior to assembly in the plastic laminate cartridge, patterned ITO electrode array microscope slides were cleaned via successive sonication in dilute ammonia (1:1 (vol.) nanopure H_2O: ammonium hydroxide), nanopure H_2O, acetone, and nanopure H_2O, for 5 min each at room temperature (22 °C). Between sonication steps the glass slides were rinsed in nanopure H_2O and dried with a stream of N_2. Following cleaning, the slides were assembled into the plastic laminate cartridge or stored in nanopure H_2O for up to 12 h.

AuNPs were electrochemically deposited onto the clean ITO working electrodes using a method modified from Wang et al.[29] To sodium phosphate buffer (10 mL of 10 mM, pH 7.0) was added $KAu(CN)_2$ (600 μL of 2.0 mM) in nanopure H_2O (end concentration 110 μM). This solution was introduced to a given three electrode cell in the ITO–glass/plastic laminate cartridge via the microfluidic channel inlet port. AuNP electrodeposition occurred by cyclic voltammetry from −0.5 to −1.4 V vs. ITO pseudo-reference at room temperature (without deoxygenation) for 20 cycles at a potential scan rate (v) of 50 mV s^{-1}. Following electrodeposition the channel was flushed with nanopure H_2O, (~3 mL) followed by a stream of air to vacate the channel.

PB was deposited onto the AuNP-modified ITO working electrode using a method modified from Qiu et al.[22] A solution with $FeCl_3$ (1.0 mM), $Fe(CN)_6^{3-}$ (1.0 mM), KCl (0.1 M), and HCl (0.025 M) in nanopure H_2O was introduced to a given three electrode cell in the ITO–glass/plastic laminate cartridge via the microfluidic channel inlet port, and incubated at room temperature for 30 min. Following deposition the channel was flushed with nanopure H_2O (~3 mL), followed by a stream of air to vacate the channel. Living cell/glycerol–silica matrix precursor solutions were introduced to the device following electrode surface functionalization.

Encapsulation of S. cerevisiae and/or E. coli in PGS Derived Silica Thin Films: For orthogonal mode biodetection, silica matrix precursor solutions were prepared by first adding an equal molar mixture of *S. cerevisiae* cells engineered to express YFP, and *S. cerevisiae* cells engineered to express and secrete GOx (total concentration 10^6–10^7 cells/mL), to sodium phosphate buffer (100 mM, pH 6.0). This cell/buffer solution was added to the PGS in a 1:1 volume ratio (final volume of 500–750 μL) in a 1.5 mL polypropylene microcentrifuge tube, and homogenized by vortexing for 60 s. The solution was aged for 30 min at room temperature (22 °C), and then transferred into the ITO–glass/plastic laminate via a syringe interfaced to an inlet port by a plastic tube (1/16 inch o.d.). By allowing the solution to age before introducing it to the device the *S. cerevisiae* cells remained homogenously dispersed throughout the silica matrix upon gelation. Otherwise, *S. cerevisiae* cells were observed to settle to the bottom of the microfluidic channel, reaching an undesirably high density on top of the ITO electrodes upon silica matrix gelation. Once loaded, the tube was removed and the inlet and outlet ports were sealed with adhesive tape. Cell/buffer/PGS solution gelation occurred less than 30 min after introduction to the device. This was confirmed by monitoring gelation of the remaining cell/buffer/PGS solution not introduced to the cartridge.

For disparate cell co-entrapment and multianalyte detection, the cell/buffer solution contained *S. cerevisiae* cells engineered to express YFP and *E. coli* cells engineered to display green fluorescence, at a ratio of approximately 1:2 (*S. cerevisiae* cells to *E. coli* cells) in sodium phosphate buffer (100 mM, pH 6.0). There was no other change to the procedure as described above.

ABTS Assay: 2,2′-Azino-bis[3-ethyl-benzothiazoline-6-sulfonic acid] (ABTS) assay, modified from Sun et al.,[30] was performed

NANO MICRO small

independently of the simultaneous fluorescence and electrochemical measurements (separate detection regions/wells and times). The ABTS working solution consisted of sodium phosphate buffer (100 mM, pH 7.0), glucose (50 mM), horseradish peroxidase (HRP, 3 units), and ABTS (2 mg/mL). Following a 9 h analyte solution treatment of the silica matrix entrapped cells beneath a given well in the ITO–glass/plastic laminate cartridge, the analyte solution was discarded and replaced with ABTS working solution (250 μL). Incubation with ABTS working solution proceeded overnight at room temperature (22 °C). The wells were then imaged with a digital camera, and ABTS solution was collected and absorbance was measured at 410 nm using a microplate UV/Vis spectrophotometer.

Electrochemical Instrumentation and Assay; Fluorescence and Scanning Electron Microscope Imaging: All electrochemical measurements were performed on a PalmSens hand-held potentiostat (Palm Instruments BV, The Netherlands) using the on-chip ITO working, ITO pseudo-reference, and ITO counter electrodes. Chronamperometric measurements (1 s potential step to −100 mV vs. ITO pseudo-reference) were performed hourly starting upon the introduction of analyte solution (YP with or without galactose at varying concentration, and glucose (50 mM)) during simultaneous fluorescence and electrochemical measurements. Fluorescence microscopy imaging was performed on a Zeiss Axiovert 200M inverted microscope (Germany) and recorded using a Zeiss monochrome high resolution camera (AxioCam HRm). SEM imaging was performed by a Hitachi 3200N scanning electron microscope operating at 25 kV.

Supporting Information

Supporting Information is available from the Wiley Online Library or from the author.

Acknowledgements

We thank Dr. David R. Wheeler (Sandia National Labs) for the concept and initial synthesis of the poly(glycerol) silicate. This work was funded by the Defense Treat Reduction Agency (DTRA) Chem. Bio. Basic Research Program (grants B084467I, B094732I, B0114453I), and the Sandia Lab Directed Research and Development (LDRD) Program. CJB acknowledges funding from the Air Force Office of Scientific Research grant FA 9550-10-1-0054, and the U.S. Department of Energy, Office of Science, Office of Basic Energy Sciences, Division of Materials Sciences and Engineering. SMB acknowledges funding from the U.S. Department of Energy National Nuclear Security Administration Office for Nonproliferation Research and Development (NA-22). Sandia National Laboratories is a multi-program laboratory operated by Sandia Corporation, a wholly owned subsidiary of Lockheed Martin Company, for the U.S. Department of Energy's National Nuclear Security Administration under contract DE-AC04-94AL85000.

[1] F. Lagarde, N. Jaffrezic-Renault, *Anal. Bioanal. Chem.* **2011**, *400*, 947–964.
[2] I. J. Allan, B. Vrana, R. Greenwood, G. A. Mills, B. Roig, C. Gonzalez, *Talanta* **2006**, *69*, 302–322.
[3] X. Xu, Y. Ying, *Food Rev. Int.* **2011**, *27*, 300–329.
[4] L. Su, W. Jia, C. Hou, Y. Lei, *Biosens. Bioelectron.* **2011**, *26*, 1788–1799.
[5] D. A. Stenger, G. W. Gross, E. W. Keefer, K. M. Shaffer, J. D. Andreadis, W. Ma, J. J. Pancrazio, *Trends Biotechnol.* **2001**, *19*. 304–309.
[6] Y. Lei, W. Chen, A. Mulchandani, *Anal. Chim. Acta* **2006**, *568*, 200–210.
[7] S. Belkin, *Curr. Opin. Microbiol.* **2003** *6*, 206–212.
[8] T. H. Rider, M. S Petrovick, F. E. Nargi, J. D. Harper, E. D. Schwoebel, R. H. Mathews, D. J. Blanchard, L. T. Bortolin, A. M. Young, J. Chen, M. A. Hollis, *Science* **2003**, *301*, 213–215.
[9] K. H. Gilchrist, L. Giovangrandi, R. H. Whittington, G. T. A. Kovacs, *Biosens. Bioelectron.* **2005**, *20*, 1397–1406.
[10] M. S. Petrovick, F. E. Nargi, T. Towle, K. Hogan, M. Bohane, D. J. Wright, T. H. MacRae, M. Potts, R. F. Helm, *Biotechnol. Bioeng.* **2010**, *106*, 474–481.
[11] C. Amatore, S. Arbault, Y. Chen, C. Crozatier, F. Lamaître, Y. Verchier, *Angew. Chem. Int. Ed.* **2006**, *45*, 4000–4003.
[12] A. Meunier, O. Jouannot, R. Fulcrand, I. Fanget, M. Bretou, E. Karatekin, S. Arbault, M. Guille, F. Darchen, F. Lemaître, C. Amatore, *Angew. Chem. Int. Ed.* **2011**, *50*, 5081–5084.
[13] X. T. Xheng, W. Hu, H. Wang, H. Yang, W. Zhou, C. M. Li, *Biosens. Bioelectron.* **2011**, *26*, 4484–4490.
[14] B.-X. Shi, Y. Wang, T.-L. Lam, W.-H. Huang, K. Zhang, Y.-C. Leung, H. L. Chan, *Biomicrofluidics* **2010**, *4*, 043009.
[15] E. S. Douglas, S. C. Hsiao, H. Onoe, C. R. Bertozzi, M. B. Francis, R. A. Mathies, *Lab Chip* **2009**, *9*, 2010–2015.
[16] K. Buonasera, G. Pezzotti, V. Scognamiglio, A. Tibuzzi, M. T. Giardi, *J. Agric. Food Chem.* **2010**, *58*, 5982–5990.
[17] J. C. Harper, D. M. Lopez, E. Larkin, M. K. Economides, S. K. McIntyre, T. M. Alan, M. S. Tartis, M. Werner-Washburne, C. J. Brinker, S. M. Brozik, D. R. Wheeler, *Chem. Mater.* **2011**, *23*, 2555–2564.
[18] T. L. Edwards, J. C. Harper, R. Polsky, D. M. Lopez, D. R. Wheeler, A. C. Allen, S. M. Brozik, *Biomicrofluidics* **2011**, *5*, 044115.
[19] R. Woods, in *Electroanalytical Chemistry* (Ed: A. Bard), Marcel Dekker, New York **1976**.
[20] A. A. Karyakin, *Electroanalysis* **2001**, *13*, 813–819.
[21] D. Ellis, M. Eckhoff, V. D. Neff, *J. Phys. Chem.* **1981**, *85*, 1225–1231.
[22] J.-D. Qiu, H.-Z. Peng, R.-P. Liang, J. Li, X.-H. Xia, *Langmuir* **2007**, *23*, 2133–2137.
[23] J. Zhang, J. Li, F. Yang, B. Zhang, X. Yang, *J. Electroanal. Chem.* **2010**, *638*, 173–177.
[24] J. R. Premkumar, E. Sagi, R. Rozen, S. Belkin, A. D. Modestov, O. Lev, *Chem. Mater.* **2002**, *14*, 2676–2686.
[25] E. Sagi, N. Hever, R. Rozen, A. J. Bartolome, J. R. Premkumar, R. Ulber, O. Lev, T. Scheper, S. Belkin, *Sens. Actuat. B-Chem.* **2003**, *90*, 2–8.
[26] S. Harbaugh, N. Kelley-Loughnane, M. Davidson, L. Narayanan, S. Trott, Y. G. Chushak, M. O. Stone, *Biomacromol.* **2009**, *10*, 1055–1060.
[27] E. K. Bomati, G. Manning, D. D. Deheyn, *BMC Evol. Biol.* **2009**, *9*, 77.
[28] T. Khonina, O. Chupakhin, L. Larionov, T. Boyakovskaya, A. Suvorov, E. Shadrina, *Pharm. Chem. J.* **2008**, *42*, 609–613.
[29] J. Wang, L. Wang, J. Di, Y. Tu, *Talanta* **2009**, *77*, 1454–1459.
[30] L. H. Sun, T. Bulter, M. Alcalde, I. P. Petrounia, F. H. Arnold, *ChemBioChem* **2002**, *3*, 781–783.

Received: February 13, 2012
Revised: March 31, 2012
Published online: June 11, 2012

